PLOS ONE

RESEARCH ARTICLE

Effect of field strength on RF power deposition near conductive leads: A simulation study of SAR in DBS lead models during MRI at 1.5 T—10.5 T

Ehsan Kazemivalipour[1,2,3,4,5], **Alireza Sadeghi-Tarakameh**[6], **Boris Keil**[7], **Yigitcan Eryaman**[6], **Ergin Atalar**[2,3], **Laleh Golestanirad**[1,8]*

1 Department of Radiology, Feinberg School of Medicine, Northwestern University, Chicago, Illinois, United States of America, **2** Electrical and Electronics Engineering Department, Bilkent University, Ankara, Turkey, **3** National Magnetic Resonance Research Center (UMRAM), Bilkent University, Ankara, Turkey, **4** Athinoula A. Martinos Center for Biomedical Imaging, Department of Radiology, Massachusetts General Hospital, Harvard Medical School, Charlestown, Massachusetts, United States of America, **5** Harvard Medical School, Boston, Massachusetts, United States of America, **6** Center for Magnetic Resonance Research (CMRR), University of Minnesota, Minneapolis, Minnesota, United States of America, **7** Institute of Medical Physics and Radiation Protection, TH Mittelhessen University of Applied Sciences, Giessen, Germany, **8** Department of Biomedical Engineering, McCormick School of Engineering, Northwestern University, Evanston, Illinois, United States of America

* Laleh.rad1@northwestern.edu

Citation: Kazemivalipour E, Sadeghi-Tarakameh A, Keil B, Eryaman Y, Atalar E, Golestanirad L (2023) Effect of field strength on RF power deposition near conductive leads: A simulation study of SAR in DBS lead models during MRI at 1.5 T—10.5 T. PLoS ONE 18(1): e0280655. https://doi.org/10.1371/journal.pone.0280655

Editor: Stephan Orzada, German Cancer Research Center: Deutsches Krebsforschungszentrum, GERMANY

Received: May 17, 2022

Accepted: January 5, 2023

Published: January 26, 2023

Data Availability Statement: All relevant data are within the manuscript and its Supporting Information files.

Funding: LG received funding from National Institute of Biomedical Imaging and Bioengineering (NIBIB) grant number: R01 EB030324 funder website: https://www.nibib.nih.gov/research-program/c3i-program YE received funding from National Institute of Biomedical Imaging and

Abstract

Background

Since the advent of magnetic resonance imaging (MRI) nearly four decades ago, there has been a quest for ever-higher magnetic field strengths. Strong incentives exist to do so, as increasing the magnetic field strength increases the signal-to-noise ratio of images. However, ensuring patient safety becomes more challenging at high and ultrahigh field MRI (i.e., $\geq$3 T) compared to lower fields. The problem is exacerbated for patients with conductive implants, such as those with deep brain stimulation (DBS) devices, as excessive local heating can occur around implanted lead tips. Despite extensive effort to assess radio frequency (RF) heating of implants during MRI at 1.5 T, a comparative study that systematically examines the effects of field strength and various exposure limits on RF heating is missing.

Purpose

This study aims to perform numerical simulations that systematically compare RF power deposition near DBS lead models during MRI at common clinical and ultra-high field strengths, namely 1.5, 3, 7, and 10.5 T. Furthermore, we assess the effects of different exposure constraints on RF power deposition by imposing limits on either the B_1^+ or global head specific absorption rate (SAR) as these two exposure limits commonly appear in MRI guidelines.

Methods

We created 33 unique DBS lead models based on postoperative computed tomography (CT) images of patients with implanted DBS devices and performed electromagnetic

Bioengineering (NIBIB) grant numbers: P41EB027061 and U01EB025144 funder website: https://www.nibib.nih.gov/research-program/c3i-program The funders had no role in study design, data collection and analysis, decision to publish, or preparation of the manuscript.

Competing interests: The authors have declared that no competing interests exist.

simulations to evaluate the SAR of RF energy in the tissue surrounding lead tips during RF exposure at frequencies ranging from 64 MHz (1.5 T) to 447 MHz (10.5 T). The RF exposure was implemented via realistic MRI RF coil models created based on physical prototypes built in our institutions. We systematically examined the distribution of local SAR at different frequencies with the input coil power adjusted to either limit the B_1^+ or the global head SAR.

Results

The MRI RF coils at higher resonant frequencies generated lower SARs around the lead tips when the global head SAR was constrained. The trend was reversed when the constraint was imposed on B_1^+.

Conclusion

At higher static fields, MRI is not necessarily more dangerous than at lower fields for patients with conductive leads. Specifically, when a conservative safety criterion, such as constraints on the global SAR, is imposed, coils at a higher resonant frequency tend to generate a lower local SAR around implanted leads due to the decreased B_1^+ and, by proxy, **E** field levels.

1 Introduction

Magnetic resonance imaging (MRI) has become a powerful imaging modality in the arsenal of noninvasive diagnostic tools, providing an unparalleled spatial resolution and soft-tissue contrast, as well as allowing to monitor functional changes in tissue. Since the advent of MRI nearly four decades ago, there has been a race toward ever-increasing magnetic fields. There are strong incentives to do so: increasing the strength of the static magnetic field substantially increases the signal-to-noise ratio to visualize small structures previously unobservable on MRI scans. For example, MRI at 7 T can differentiate subsegments of the globus pallidus, a small brain nucleus that is the target of neuromodulation therapies, such as deep brain stimulation (DBS) [1].

With MRI becoming increasingly prevalent, the number of cases in which patients with conductive implants are referred for an MRI exam increases. It is estimated that 50% to 75% of patients with cardiovascular implants or neuromodulation devices will require MRI during their lifetime [2, 3], with many patients requiring repeated examinations [4]. Nevertheless, performing MRI in the presence of electronic implants that typically have elongated conductive leads is still challenging due to the risks associated with the radio frequency (RF) heating of implants. This phenomenon, commonly known as the *antenna effect*, occurs when the electric field of the MRI transmit coil induces current on conductive lead wires, which raises the specific absorption rate (SAR) of the RF energy in the tissue surrounding the lead tips [5–7]. Excessive tissue heating and serious thermal injuries could arise from this mechanism [8]. Therefore, the criteria under which patients with conductive implants are indicated for MRI are restrictive. Most patients with DBS devices, for example, can only undergo MRI at 1.5 T scanners with pulse sequences with substantially reduced power which are not optimal for target visualization [9–11].

Extensive effort has been dedicated to assessing RF heating of elongated implants during MRI at 1.5 T and, to a lesser degree, at 3 T and above [12]. However, a comparative study examining the differential effects of resonant frequency on implant heating in the wide range

of currently available MRI systems is missing. This study is particularly important as misconceptions exist among some MRI users that scanners at higher field strengths are inherently more dangerous in terms of local implant heating.

We report the results of a systematic simulation study with 33 patient-derived models of DBS leads exposed to RF radiation in a range of frequencies corresponding to 1.5 to 10.5 T MRI and compare the local SAR around the lead tips for different exposure limits. Because the trajectory of an implanted lead substantially affects local power deposition near the lead's tip [13–17] and because we aimed to generate data representative of the clinical population, lead models have trajectories reconstructed from computed tomography (CT) images of patients with DBS devices. Moreover, models of MRI RF coils were recreated based on physical prototypes that we have built for neuroimaging studies; thus, their field distributions represent realistic scenarios. We evaluated the maximum of a 1 g-averaged SAR in cubic volumes surrounding the tips of DBS lead models for exposure conditions that put a cap on a) the magnitude of B_1^+ and b) the magnitude of the global head SAR (GHSAR). These two exposure constraints were selected as they are commonly found in the MRI-conditional labeling of devices. Older guidelines imposed the limit on the global SAR, which tends to be more conservative, whereas recent guidelines impose limits on B_1^+.

2 Methods

All models described below are available to be used for research upon sending written request to the corresponding author.

2.1 RF transmit coils

Coil geometries were based on physical prototypes built in our labs. Four RF transmit head coil models were constructed and tuned to respective proton Larmor frequencies at 1.5, 3, 7, and 10.5 T (64 MHz for 1.5 T, 127 MHz for 3 T, 297 MHz for 7 T, and 447 MHz for 10.5 T). These models included two 16-rung low-pass birdcage coils at 1.5 T [18] and 3 T [19], a 16-rung shielded hybrid birdcage coil at 7 T [20] and an 8-channel bumped dipole array at 10.5 T [21]. Fig 1 presents the geometrical details of the coils loaded with a homogeneous human head model.

The 1.5, 3, and 7 T birdcage coils were excited using two ports, each fed with the same amplitude and a 90˚ phase difference to achieve circular polarization (CP mode) in the sample. The 8-channel bumped dipole 10.5 T coil was excited using eight ports, each fed with the same amplitude and a 45˚ phase difference to create a CP-like mode. S1 Fig displays B_1^+ and **E** field distributions on an axial plane passing through the iso-center of each coil. As observed, the B_1^+ uniformity in the CP excitation mode was decreased by increasing the field strength. This outcome was expected due to the lower ratio of the RF wavelength to the body model dimensions at higher field strengths [22, 23].

2.2 DBS lead models with realistic trajectories

It is established that the trajectory of an elongated lead and its position within the MRI coil strongly affects its RF heating [24–30]. The extracranial DBS lead trajectories (i.e., the trajectory of the portion of the lead that is outside of the brain and placed over the skull) vary substantially from patient to patient, depending on the surgeon's practice styles. Thus, studies that aim to assess RF heating of DBS implants should ideally include clinically relevant lead trajectories reflective of the heterogeneity observed in the patient population. In this study, we simulated 33 unique DBS lead models with realistic patient-derived trajectories based on postoperative CT images of 20 patients operated in our institutions. Use of patient data for the

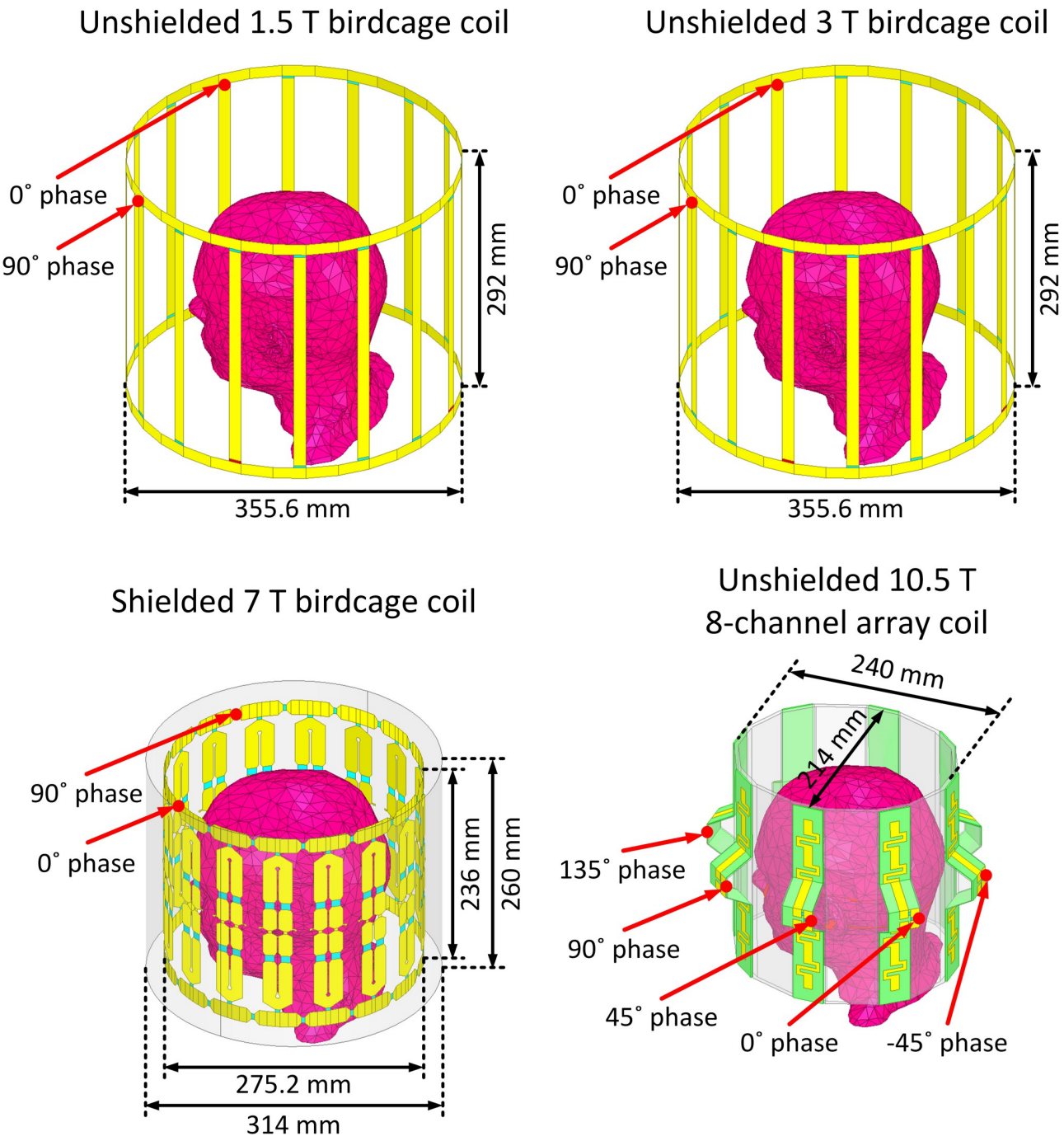

Fig 1. Numerical models of a 1.5 T 16-rung low-pass birdcage coil tuned at 64 MHz, a 3 T 16-rung low-pass birdcage coil tuned at 127 MHz, a 7 T 16-rung hybrid birdcage coil tuned at 297 MHz, and a 10.5 T 8-channel bumped dipole array tuned at 447 MHz all loaded with a homogeneous human head model with no implant. The geometrical dimensions of the coils were the same as the coils reported in literature [18–21].

https://doi.org/10.1371/journal.pone.0280655.g001

purpose of MRI RF heating assessment and publication of de-identified images was approved by Northwestern University's Institutional Review Board (STU00206859). Consent was waived as the data was collected retrospectively and analyzed anonymously. The details of image segmentation and model creation were similar to our previous studies [13, 31–33].

Out of the 33 simulated lead models, 26 models were constructed based on the CT images of patients with bilateral leads (ID1 –ID13, Fig 2) and 7 models were constructed based on the CT images of patients with unilateral leads (ID14 –ID20, Fig 2). Each lead model comprised four electrode contacts connected via a solid straight platinum core (diameter = 0.26 mm and $\sigma = 9.3\times10^6$ S/m), embedded in a urethane insulator (diameter = 1.27 mm and $\varepsilon_r = 3.5$). All lead models were 40 cm long. Lead models were incorporated into a homogeneous human head model with the properties of average tissue ($\sigma = 0.49$ S/m and $\varepsilon_r = 66$). Note that our models represent lead-only DBS systems, that is, extension cables (~ 60 cm) and the pulse generator were not included. Also, note that we chose to keep the dielectric properties of the tissue constant over the range of studied frequencies.

2.3 Numerical simulation

Electromagnetic (EM) simulations were implemented in ANSYS Electronics Desktop 2019 R2 (ANSYS Inc., Canonsburg, PA) on a Dell PowerEdge R740xd server equipped with two Intel (R) Xeon(R) Gold 6140 2.3 GHz processors and 1.5 TB of RAM. The EM fields induced in the head and lead models by each coil were computed using a numerical method based on the combined FEM simulation and circuit analysis [13, 19–37]. The maximum of 1 g-averaged

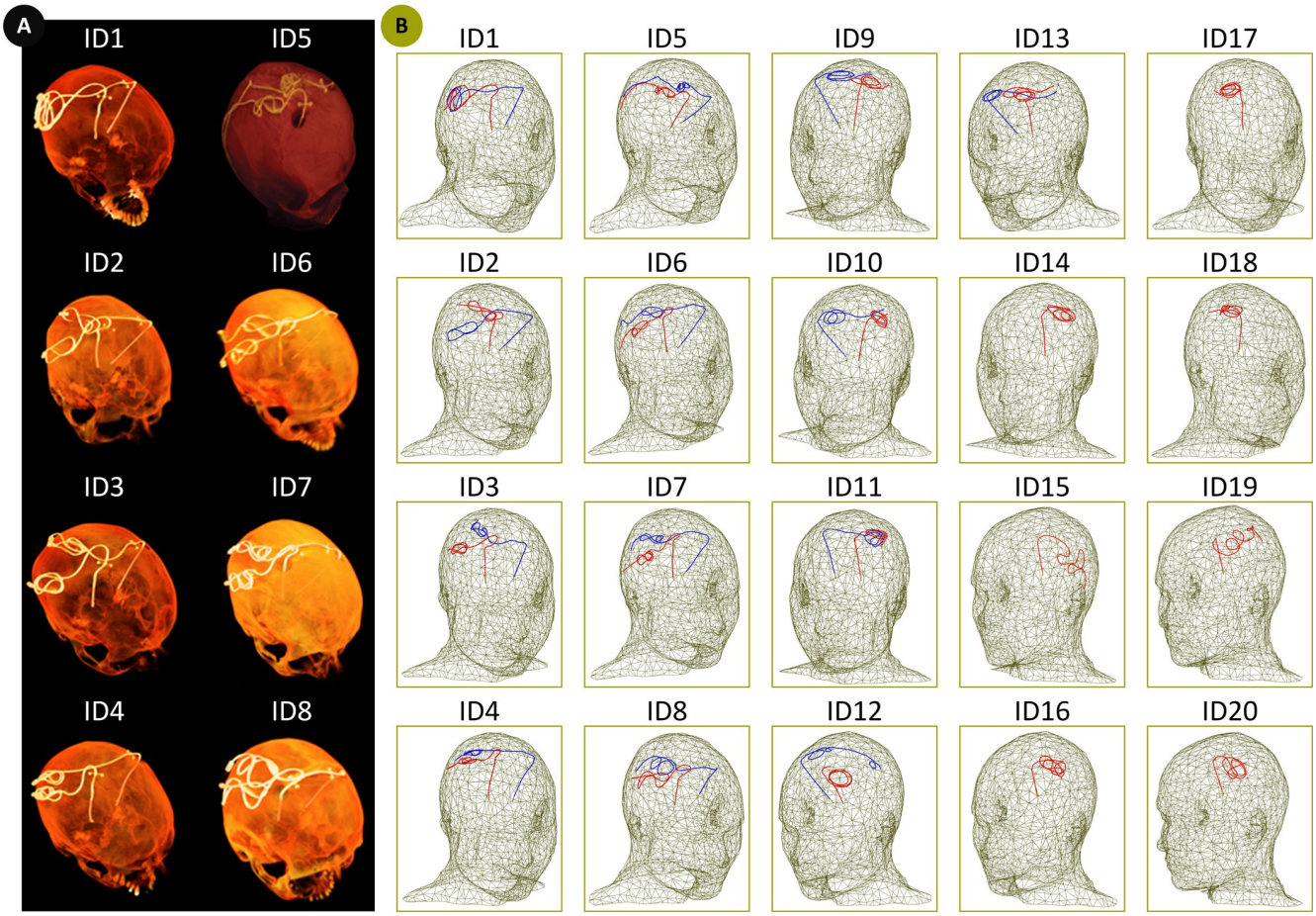

Fig 2. (A) Examples of postoperative CT images (ID1-ID8). (B) Reconstructed models of isolated DBS leads (ID1—ID20). Lead trajectories were constructed based on the postoperative CT images of 13 patients with bilateral DBS implantations (ID1—ID13), and 7 patients with unilateral DBS implantations (ID14—ID20) and were incorporated in a homogeneous head model for EM simulations.

https://doi.org/10.1371/journal.pone.0280655.g002

SAR (1 g-SAR_{max}) was calculated within a high mesh resolution cubic volume of 20 × 20 × 20 mm surrounding the DBS lead contacts (referred to as the SAR box). As a reminder, the point-wise local SAR is defined as follows:

$$SAR = \frac{1}{2\rho}\sigma||E||^2, \quad (1)$$

where $||E||$ denotes the magnitude of the electric field (V/m), ρ is the mass density of the material (kg/m^3), and σ represents the material conductivity (S/m). The averaged SAR is calculated over a volume that surrounds each mesh point. The volume used in the 1 g estimation is determined at each mesh point by a closed surface with a volume such that the sum of the product of each material subvolume within totals 1 g by its mass density.

For each coil, we adjusted the input power to impose limits on 1) the GHSAR (3 W/kg) and (2) spatial average of B_1^+ on an axial plane passing through the center of the head (B_1^+ = 2 μT). These two outcome measures were chosen because they are automatically calculated and reported by the scanner and are commonly adopted in MRI-conditional guidelines. The plane over which $B_1^+$was sampled was 40 mm below the coil isocenters, allowing unbiased B_1^+ averaging without implant-induced perturbations (Fig 3).

For all simulations, the edge length of the tetrahedral mesh elements inside the head model was confined to <10 mm, except for the SAR boxes, which enforced the edge lengths to <1 mm. In addition, the triangular mesh edge lengths on the surfaces of all electrodes and their insulation were restricted to <0.5 mm. Finally, the maximum size of the mesh elements on the RF coil components was set to <5 mm, except for the lumped ports, in which the maximum element length was restricted to <1 mm. The ANSYS high-frequency structure simulator was set to follow an adaptive meshing process, where the mesh was refined until the magnitude of the difference between the scattering parameters calculated in two consecutive iterations was less than 0.01. We demonstrated that the convergence criteria based on the S-parameters also guarantees the convergence of the electric field (and SAR) around the implanted leads [38]. All simulations converged within three adaptive passes. The simulation time was ~12 hours for each model.

Fig 3 presents examples of the mesh density on the surface of leads, their insulation, and SAR boxes at 3 T for a representative patient with bilateral leads (ID12). Fig 3 also depicts the 1 g-SAR distribution on a plane passing through the lead tips and the B_1^+ distribution on an axial plane passing through the center of the head when the coil inputs are adjusted to maintain the GHSAR at 3 W/kg.

3 Results

Fig 4 displays an example of the distribution of the 1 g-SAR on an axial plane passing through distal electrode contacts for each of the two exposure limits (patient ID12). The box plots presenting the 1 g-SAR_{max}, mean of B_1^+, and mean of $||\mathbf{E}||$ for all lead models are provided in Fig 5 (B_1^+ and $||\mathbf{E}||$ are averaged over an axial plane passing through the center of the head shown in Fig 3). When the input power of the coils was adjusted to generate a GHSAR of 3 W/kg, the 1 g-SAR_{max} (mean ± standard deviation) was 104 ± 99 W/kg at 1.5 T, 32 ± 30 W/kg at 3 T, 19 ± 15 W/kg at 7 T, and 29 ± 17 W/kg at 10.5 T (S1 Table). A one-way repeated measure analysis of variance (ANOVA) was conducted on lead models to examine the effects of different field strengths on RF power deposition near the lead tip. The results revealed that when the GHSAR was fixed, the variation of the field strength and resonant frequency led to statistically significant differences in power deposition near the lead tip ($F(3, 96) = 24.09$, $p < 1.04$ E-11). A post-hoc pairwise comparison test revealed that, for a fixed GHSAR, local SAR at 1.5 T was

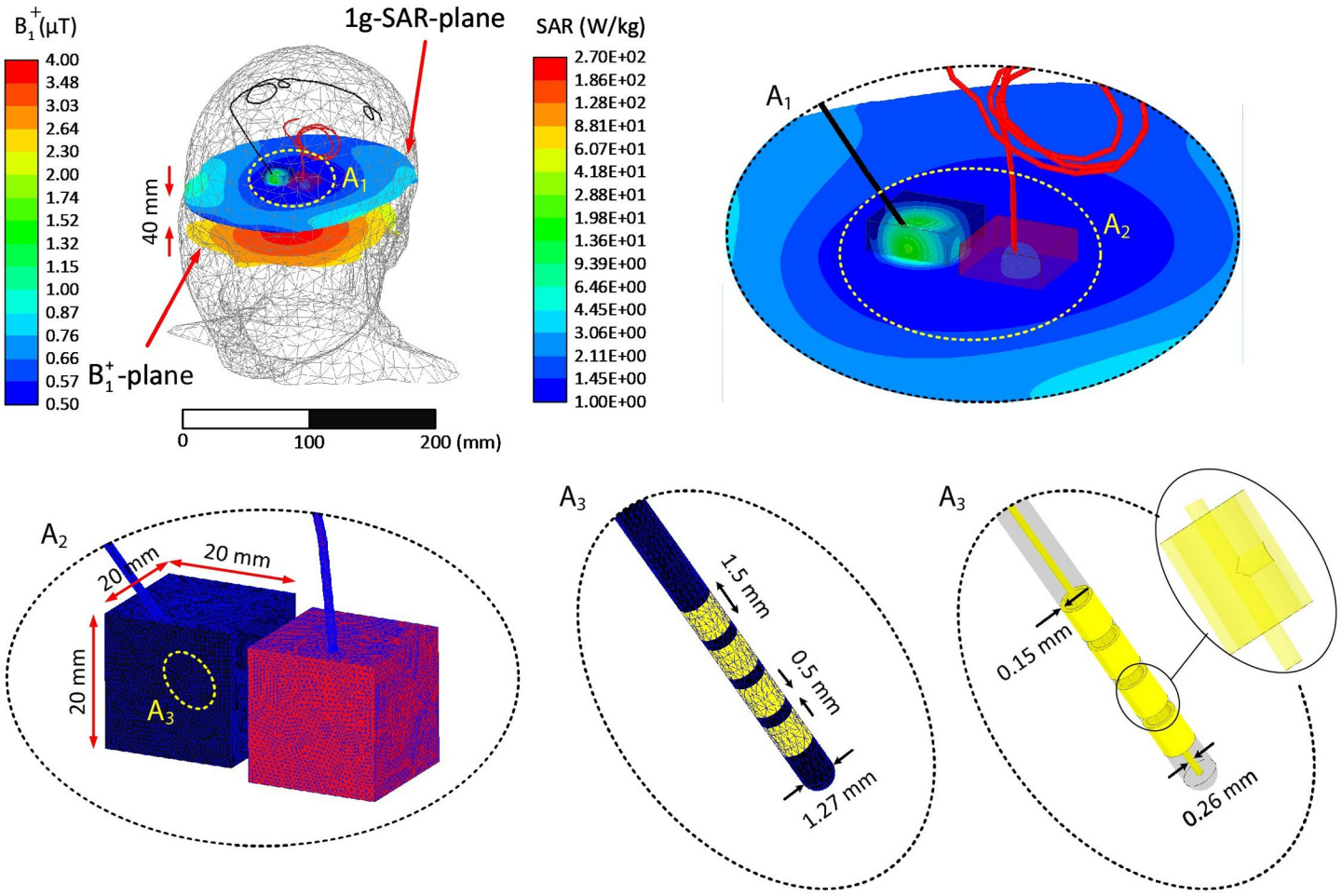

Fig 3. Example of mesh density in the lead, insulation, and SAR boxes of a representative patient (ID12) at 3 T. A1: Closeup view of leads withing the high-resolution mesh regions. A2-A3: Schematic of mesh in the cubic area surrounding the lead tips and on the lead electrodes. A3: View of interconnections between electrodes and the central core. The coil's input power was adjusted to generate a GHSAR of 3 W/kg. The distribution of 1g-SAR on a plane passing through the lead tips, the distribution of B_1^+ on an axial plane passing through the patient's forehead, and the lead's contacts' geometrical details are also presented.

https://doi.org/10.1371/journal.pone.0280655.g003

significantly higher than SAR at all other field strengths ($p < .001$ compared to 3, 7, and 10.5 T). Moreover, SAR at 3 T was significantly higher than that at 7 T ($p = .008$) but not significantly different from SAR at 10.5 T ($p = .54$). Finally, local SAR at 7 T was significantly lower than that at all other field strengths ($p = .001$ compared to 10.5 T).

When the output power was adjusted to generate a mean $B_1^+ = 2\ \mu T$ at the center of the head, the 1 g-SAR_{max} was 13 ± 12 W/kg for the 1.5 T coil, 17 ± 16 W/kg for the 3 T coil, 29 ± 24 W/kg for the 7 T coil, and 51 ± 31 W/kg for the 10.5 T coil (see S1 Table). A one-way repeated measure ANOVA indicated that when the mean B_1^+ was fixed, the variation of the field strength/resonant frequency led to statistically significant differences in local SAR. A post-hoc pairwise comparison test confirmed a monotonous increase in the mean of local SAR as the field strength increased. For a fixed B_1^+, SAR was significantly lower at 1.5 T than that at all other field strengths ($p = .02$ compared to 3 T and $p < .001$ compared to 7 T and 10.5 T). In addition, SAR at 3 T was significantly lower than that at 7 T ($p = .003$) and 10.5 T ($p < .001$), and SAR at 7 T was significantly lower than that at 10.5 T ($p < .001$).

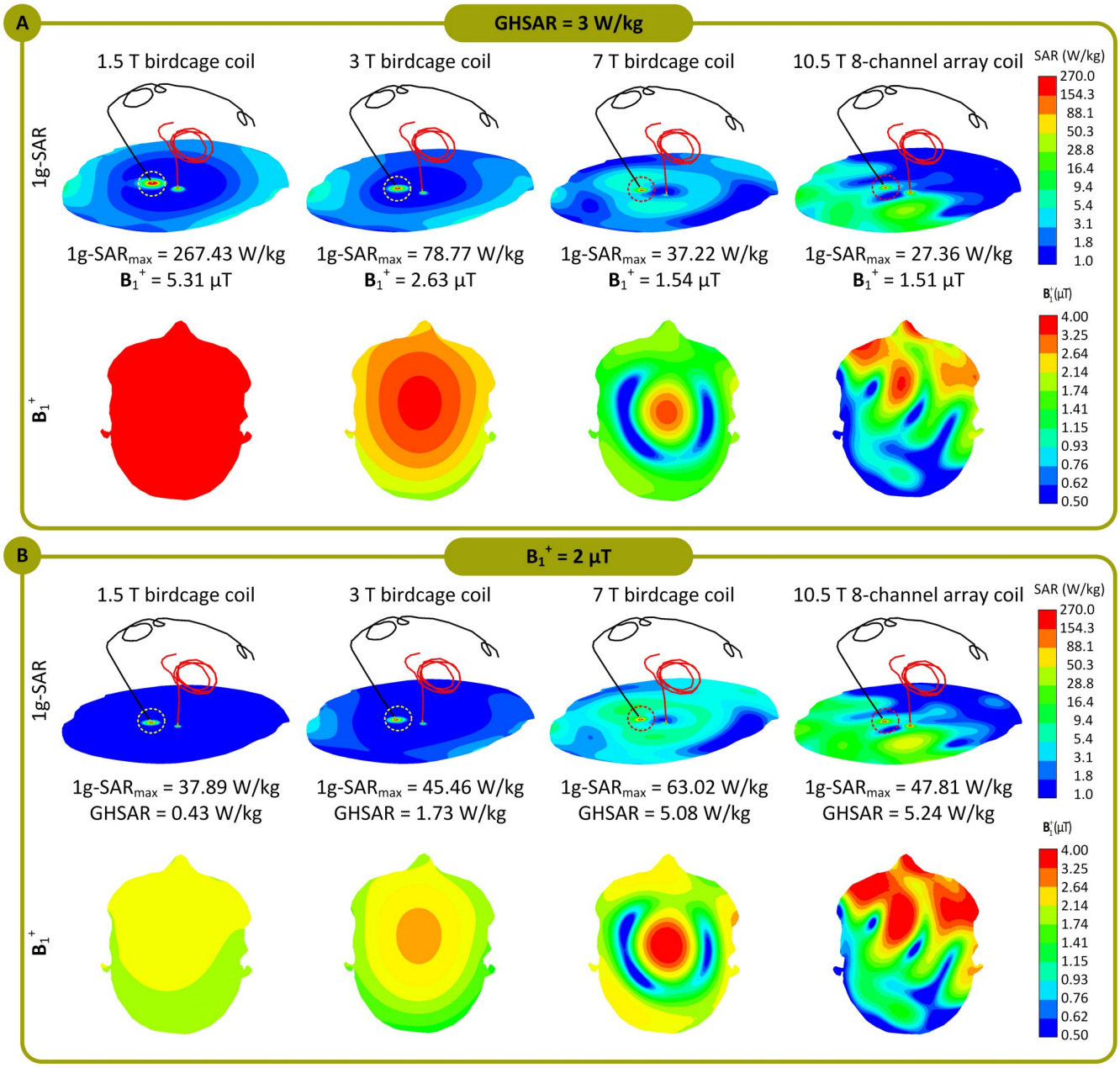

Fig 4. 1g-SAR distributions in patient 12 (ID12) for the 1.5 T, 3 T, 7 T, and 10.5 T coils over an axial plane passing through the electrode contacts. The coils' input powers are adjusted (A) to generate a GHSAR of 3 W/kg and (B) to generate an average of $B_1^+ = 2$ μT over an axial plane passing through the patient's forehead. The B_1^+ field distributions over the mentioned axial plane, which passes through the patient's forehead, are also presented. Additionally, 1g-SAR_{max}, the average of B_1^+ field, and GHSAR are also reported for all four coils.

https://doi.org/10.1371/journal.pone.0280655.g004

4 Discussion and conclusions

The market for active implantable medical devices is increasing rapidly due to the aging population and rising prevalence of chronic diseases [39]. As MRI is now the standard imaging modality for various neurological, cardiovascular, and musculoskeletal disorders, the instances in which patients with electronic implants are indicated for MRI are also rapidly increasing. Currently, RF heating caused by the interaction between MRI RF fields and the conductive

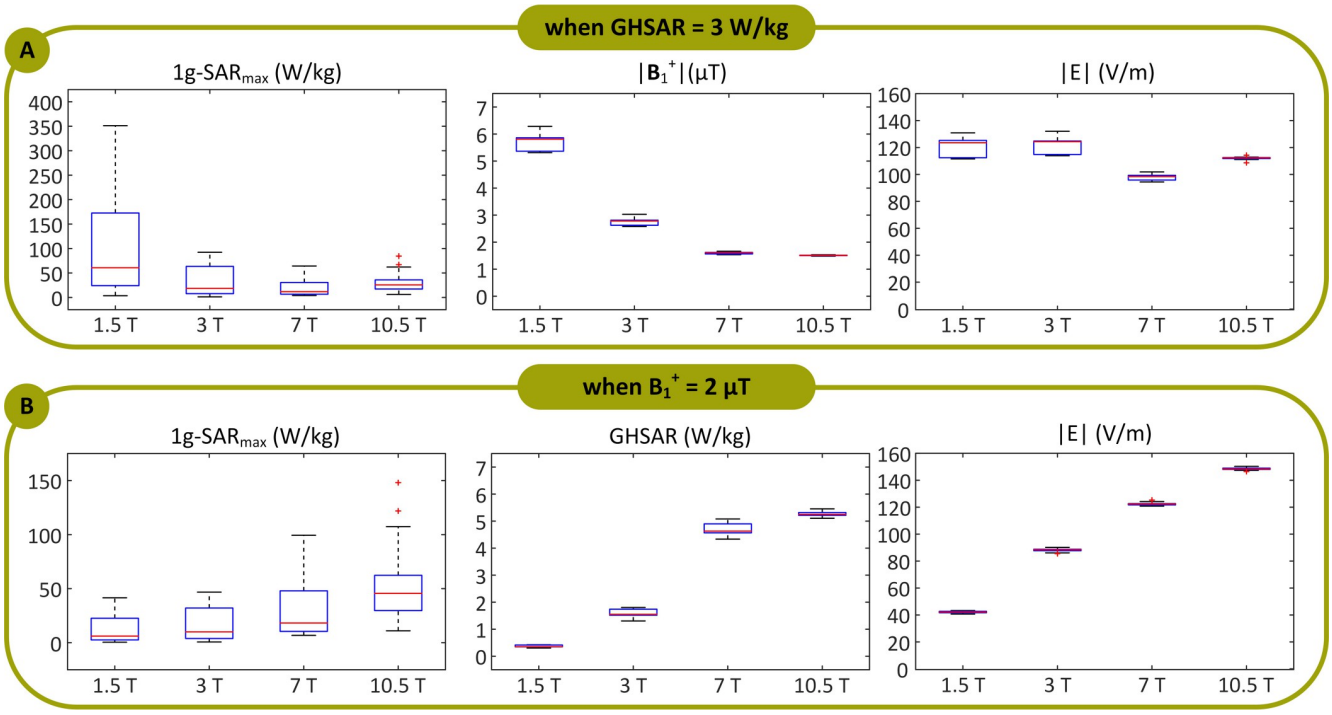

Fig 5. 1g-SAR$_{max}$, B$_1^+$, and ||*E*|| when the coils' input powers were balanced to produce a global head SAR (GHSAR) of 3 W/kg, and (B) 1g-SAR$_{max}$ and GHSAR when the coils' input powers were adjusted to generate an average of B$_1^+$ = 2 μT, over all 33 DBS lead models for the 1.5 T, 3 T, 7 T, and 10.5 T coils. Box and whisker plots display the range, median, and interquartile range (IQR) of the data. Each outlier was specified with a red '+' symbol.

https://doi.org/10.1371/journal.pone.0280655.g005

leads of active implants is the major safety concern preventing patients with electronic implants from accessing MRI. The issue is a complicated multivariable problem involving several interplaying factors, including the implant configuration and position within the patient's body [16, 40, 41] and anatomy and the position inside the RF coil [37, 42, 43], the orientation and phase of the incident electric fields [34, 44–46], and the RF transmit operating frequency [6, 38].

Over the past two decades, numerous studies have investigated RF heating of elongated implants during MRI at mid-field strength, namely 1.5 T. In contrast, scarce data exist on how increasing the magnetic field strength and, by proxy, the resonant frequency affects implant heating. We conducted a systematic simulation study to compare local SAR near DBS lead tips in a range of resonant frequencies corresponding to 1.5 T to 10.5 T MRI. Historically, MR-Conditional labels of implantable devices have imposed limitations on the global SAR, which could be either the head SAR in the case of brain implants or the total body SAR in the case of implants in the torso and abdomen. Selection of global SAR as outcome measure was primarily because the global SAR was (and still is) automatically calculated and reported by all scanners. The first MR-Conditional guidelines for DBS devices, for example, limited the GHSAR to 0.1 W/kg instead of the 3.2 W/kg, which is the FDA recommended limit for scanning in the absence of implants [47]. Recent guidelines offer the option to cap either B$_1^+$ (for newer scanners that report B$_1^+$rms) or the global SAR as previously indicated. However, although calculation of B$_1^+$ may be straightforward at lower frequencies where the field is spatially homogeneous, there are open questions as how to quantify RMS B$_1^+$ at field strengths $\geq$ 7 T where the RF field is substantially less homogenous. The issue is even more pressing in the presence of implants, as they can affect the coil's loading much more severely at

higher fields. Fig 6 gives the B_1^+ maps of all four coils in a head model without any implant (top row), and in a head model with a DBS lead (bottom row). As it can be observed, the field becomes increasingly more inhomogeneous at higher fields when the implant is present.

In general, imposing the global SAR limit is more conservative. Specifically, Fig 5 demonstrates that one needs to settle for a lower B_1^+ magnitude at higher resonant frequencies to adhere to the GHSAR limit. This result is predictable, considering that the SAR is proportional to $||E||^2$ (see Eq 1) and that Maxwell's equations state the following:

$$\nabla \times \boldsymbol{E} = -\frac{\partial \boldsymbol{B}}{\partial t}. \tag{2}$$

Therefore, capping the GHSAR keeps the magnitude of the **E** field relatively constant over the range of resonant frequencies by reducing the magnitude of B_1^+ at higher frequencies. The local RF heating generated at the lead tips is due to the current induced in the lead wires due to capacitive coupling with the **E** field and the inductive coupling with B_1^+. Therefore, for a constant GHSAR, scanners at lower resonant frequencies tend to generate higher local heating at the tips of implanted leads. In contrast, when the magnitude of B_1^+ is constant over the range of resonant frequencies, coils with higher resonant frequencies generate a higher **E** field according to Eq 2, leading to a higher local SAR around the implanted leads.

This work has several limitations. First, we have used simplified DBS lead geometries with a straight internal core, as opposed to clinically available leads which have multiple helical wires each connecting to one electrode contact. Leads with helical cores will have different electric length than their apparent length, that is, a helical lead with a 40-cm apparent length may have substantially longer internal wires. It is hard to isolate the effect of the length as it also affects the trajectory (i.e., leads with different apparent length inevitably follow different trajectories),

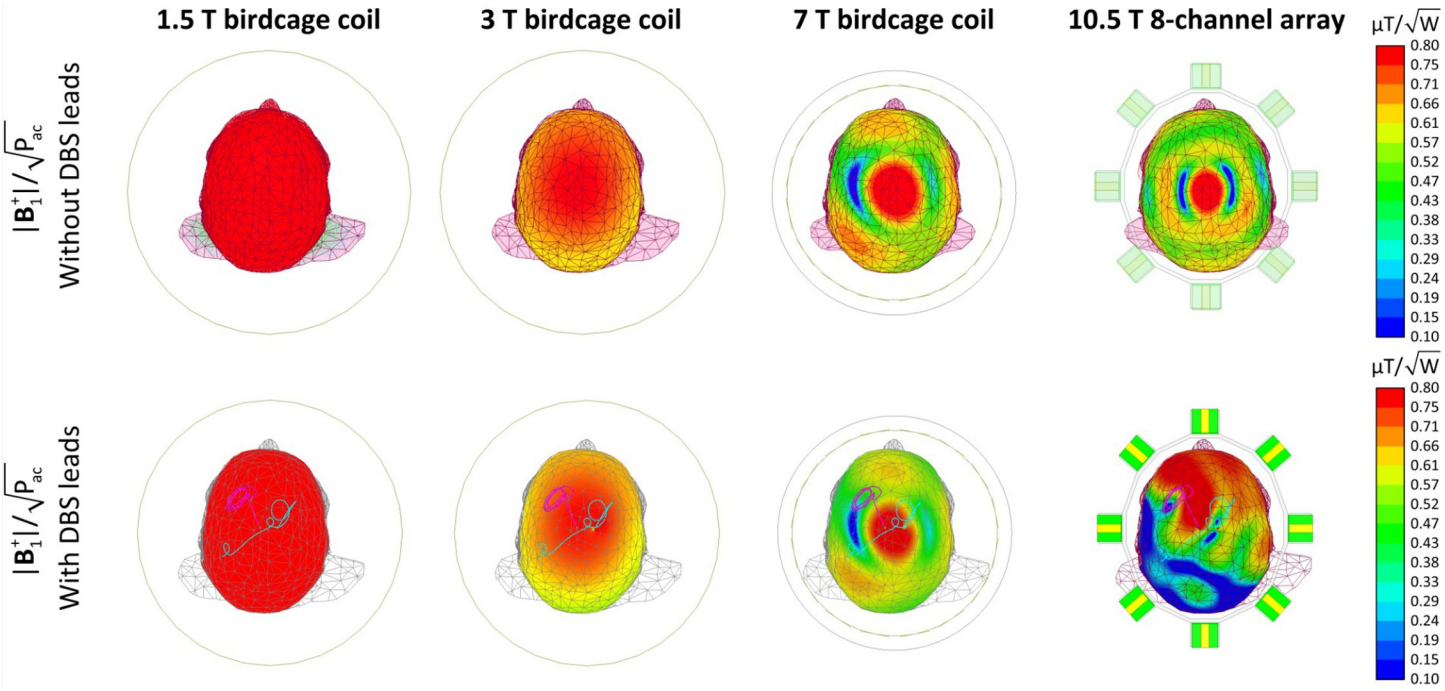

Fig 6. Normalized B_1^+ maps of the 1.5 T, 3 T, 7 T and 10.5 T coils on an axial plane passing through the iso-center in human head model with no implants (top rows) and with implants (bottom row). All four coils are driven in the CP excitation mode, where their inputs are adjusted to keep the accepted power (Pac) as 1 W. The B_1^+ maps of the second row were acquired for patient 12 (ID12).

https://doi.org/10.1371/journal.pone.0280655.g006

as well as the phenomenology of coupling with electric field (i.e., leads with helical interwire of different pitch will have different distributed inductance that could affect their resonance length). More study is needed with leads of different length and structure to better assess the effect of length. Furthermore, our models represent lead-only DBS systems. In a fully implanted device leads are connected to an extension cable (~60 cm) which is then routed along the neck toward a pulse generator implanted in the chest. Although a fully implanted system will have a longer length, our simulation result of a heterogenous dispersive body model implanted with a full DBS system showed a similar trend in SAR and B_1^+ (See S1 File). Also, we did not correct for B_1^+ field inhomogeneity at field strengths above 7 T which may happen in practice, and we did not adopt a head model with frequency dependent electric properties. The latter could specifically affect high frequency coils, as a higher frequency dependent conductivity can reduce coil coupling due to larger tissue losses. Finally, low, and ultra-low scanners (e.g., at 0.55 T and 65 mT) are absent from the current study but should be considered in future investigations especially as they are more likely to be used for implant imaging. Regardless of these limitations, this work presents the first systematic study of effect of field strength on RF heating of elongated leads. Our results agree with recent studies that compared RF heating of DBS devices across 1.5 T and 3 T scanners [48, 49] and provide useful information for a comparative evaluation of RF risks across a wide range of field strengths to help selecting appropriate safety criteria.

Supporting information

S1 Fig. B_1^+ and E field distributions on an axial plane passing through the iso-center of each coil.
(PNG)

S1 Table. Mean and standard deviation of the maximum of 1g-SAR for different coils when the input power of the coil was adjusted to generate either a $B_1^+ = 2$ μT or a GHSAR of 3 W/kg.
(DOCX)

S1 File. Analysis of heterogenous tissue.
(DOCX)

Author Contributions

Conceptualization: Ehsan Kazemivalipour, Laleh Golestanirad.

Data curation: Ehsan Kazemivalipour.

Formal analysis: Laleh Golestanirad.

Methodology: Alireza Sadeghi-Tarakameh, Boris Keil, Yigitcan Eryaman, Laleh Golestanirad.

Resources: Alireza Sadeghi-Tarakameh, Boris Keil, Yigitcan Eryaman, Ergin Atalar.

Writing – original draft: Ehsan Kazemivalipour, Laleh Golestanirad.

Writing – review & editing: Yigitcan Eryaman, Ergin Atalar, Laleh Golestanirad.

References

1. Maruyama S, Fukunaga M, Fautz HP, Heidemann R, Sadato N. Comparison of 3T and 7T MRI for the visualization of globus pallidus sub-segments. Sci Rep. 2019; 9(1):18357. Epub 2019/12/05. https://doi.org/10.1038/s41598-019-54880-x PMID: 31797993; PubMed Central PMCID: PMC6892946.

2. Kalin R, Stanton MS. Current clinical issues for MRI scanning of pacemaker and defibrillator patients. Pacing and clinical electrophysiology. 2005; 28(4):326–8. https://doi.org/10.1111/j.1540-8159.2005.50024.x PMID: 15826268

3. Falowski S, Safriel Y, Ryan MP, Hargens L. The rate of magnetic resonance imaging in patients with deep brain stimulation. Stereotactic and Functional Neurosurgery. 2016; 94(3):147–53. https://doi.org/10.1159/000444760 PMID: 27245875

4. Naehle CP, Zeijlemaker V, Thomas D, Meyer C, Strach K, Fimmers R, et al. Evaluation of cumulative effects of MR imaging on pacemaker systems at 1.5 Tesla. Pacing and clinical electrophysiology. 2009; 32(12):1526–35. https://doi.org/10.1111/j.1540-8159.2009.02570.x PMID: 19793358

5. Rezai AR, Finelli D, Nyenhuis JA, Hrdlicka G, Tkach J, Sharan A, et al. Neurostimulation systems for deep brain stimulation: In vitro evaluation of magnetic resonance imaging-related heating at 1.5 tesla. J Magn Reson Imaging. 2002; 15(3):241–50. https://doi.org/10.1002/jmri.10069 PubMed PMID: WOS:000174759500003. PMID: 11891968

6. Bhusal B, Keil B, Rosenow J, Kazemivalipour E, Golestanirad L. Patient's body composition can significantly affect RF power deposition in the tissue around DBS implants: ramifications for lead management strategies and MRI field-shaping techniques. Phys Med Biol. 2021; 66(1):015008. Epub 2020/11/26. https://doi.org/10.1088/1361-6560/abcde9 PMID: 33238247.

7. Kazemivalipour E, Vu J, Lin S, Bhusal B, Thanh Nguyen B, Kirsch J, et al. RF heating of deep brain stimulation implants during MRI in 1.2 T vertical scanners versus 1.5 T horizontal systems: A simulation study with realistic lead configurations. Annu Int Conf IEEE Eng Med Biol Soc. 2020; 2020:6143–6. https://doi.org/10.1109/EMBC44109.2020.9175737 PMID: 33019373.

8. Henderson JM, Tkach J, Phillips M, Baker K, Shellock FG, Rezai AR. Permanent neurological deficit related to magnetic resonance imaging in a patient with implanted deep brain stimulation electrodes for Parkinson's disease: case report. Neurosurgery. 2005; 57(5):E1063; discussion E. Epub 2005/11/15. https://doi.org/10.1227/01.neu.0000180810.16964.3e PMID: 16284543.

9. Medtronic. MRI guidelines for Medtronic deep brain stimulation systems. Minneapolis, MN: Medtronic; 2015. Available from http://mriquestions.com/uploads/3/4/5/7/34572113/dbs_medtronics_contrib_228155.pdf.

10. St. Jude Medical. MRI procedure information for St. Jude Medical MR conditional deep brain stimulation system. Plano, TX: St. Jude Medical; 2018. Available from https://manuals.sjm.com/~/media/manuals/product-manual-pdfs/d/6/d6db9679-aaa7-4e22-b1e3-1d8a2ac43b98.

11. Boston Scientific. ImageReady MRI Guidelines for Boston Scientific Deep Brain Stimulation System; 2019. Available from https://bostonscientific.com/content/dam/Manuals/us/current-rev-en/92195369-01_ImageReady%E2%84%A2_MRI_Guidelines_for_Boston_Scientific_Deep_Brain_Stimulation_Systems_en-US_s.pdf.

12. Bhusal B, Stockmann J, Guerin B, Mareyam A, Kirsch J, Wald LL, et al. Safety and image quality at 7T MRI for deep brain stimulation systems: Ex vivo study with lead-only and full-systems. Plos one. 2021; 16(9):e0257077. https://doi.org/10.1371/journal.pone.0257077 PMID: 34492090

13. Golestanirad L, Angelone LM, Iacono MI, Katnani H, Wald LL, Bonmassar G. Local SAR near deep brain stimulation (DBS) electrodes at 64 and 127 MHz: A simulation study of the effect of extracranial loops. Magn Reson Med. 2017; 78(4):1558–65. https://doi.org/10.1002/mrm.26535 PubMed PMID: WOS:000411186100033. PMID: 27797157

14. Nguyen BT, Pilitsis J, Golestanirad L. The effect of simulation strategies on prediction of power deposition in the tissue around electronic implants during magnetic resonance imaging. Physics in Medicine and Biology. 2020; 65(18). PubMed PMID: WOS:000573531000001. https://doi.org/10.1088/1361-6560/abac9f PMID: 32756027

15. Golestanirad L, Rahsepar AA, Kirsch JE, Suwa K, Collins JC, Angelone LM, et al. Changes in the specific absorption rate (SAR) of radiofrequency energy in patients with retained cardiac leads during MRI at 1.5T and 3T. Magn Reson Med. 2019; 81(1):653–69. PubMed PMID: WOS:000454009000054. https://doi.org/10.1002/mrm.27350 PMID: 29893997

16. Nordbeck P, Weiss I, Ehses P, Ritter O, Warmuth M, Fidler F, et al. Measuring RF-Induced Currents Inside Implants: Impact of Device Configuration on MRI Safety of Cardiac Pacemaker Leads. Magn Reson Med. 2009; 61(3):570–8. PubMed PMID: WOS:000263608300009. https://doi.org/10.1002/mrm.21881 PMID: 19132759

17. Mattei E, Triventi M, Calcagnini G, Censi F, Kainz W, Mendoza G, et al. Complexity of MRI induced heating on metallic leads: experimental measurements of 374 configurations. Biomed Eng Online. 2008; 7:11. Epub 2008/03/05. https://doi.org/10.1186/1475-925X-7-11 PMID: 18315869; PubMed Central PMCID: PMC2292730.

18. Golestanirad L, Kazemivalipour E, Keil B, Downs S, Kirsch J, Elahi B, et al. Reconfigurable MRI coil technology can substantially reduce RF heating of deep brain stimulation implants: First in-vitro study of

RF heating reduction in bilateral DBS leads at 1.5 T. Plos One. 2019; 14(8). doi: ARTN e0220043 PubMed PMID: WOS:000484999400010. https://doi.org/10.1371/journal.pone.0220043 PMID: 31390346

19. Golestanirad L, Kirsch J, Bonmassar G, Downs S, Elahi B, Martin A, et al. RF-induced heating in tissue near bilateral DBS implants during MRI at 1.5 T and 3T: The role of surgical lead management. Neuroimage. 2019; 184:566–76. https://doi.org/10.1016/j.neuroimage.2018.09.034 PubMed PMID: WOS:000449385000048. PMID: 30243973

20. Golestanirad L, Angelone LM, Kirsch J, Downs S, Keil B, Bonmassar G, et al. Reducing RF-Induced Heating Near Implanted Leads Through High-Dielectric Capacitive Bleeding of Current (CBLOC). Ieee T Microw Theory. 2019; 67(3):1265–73. https://doi.org/10.1109/TMTT.2018.2885517 PubMed PMID: WOS:000460660900041. PMID: 31607756

21. Sadeghi-Tarakameh A, DelaBarre L, Lagore RL, Torrado-Carvajal A, Wu XP, Grant A, et al. In vivo human head MRI at 10.5T: A radiofrequency safety study and preliminary imaging results. Magn Reson Med. 2020; 84(1):484–96. https://doi.org/10.1002/mrm.28093 PubMed PMID: WOS:000497604000001. PMID: 31751499

22. Webb AG, Collins CM. Parallel Transmit and Receive Technology in High-Field Magnetic Resonance Neuroimaging. Int J Imag Syst Tech. 2010; 20(1):2–13. PubMed PMID: WOS:000275024500002.

23. Collins CM, Liu W, Swift BJ, Smith MB. Combination of optimized transmit arrays and some receive array reconstruction methods can yield homogeneous images at very high frequencies. Magn Reson Med. 2005; 54(6):1327–32. PubMed PMID: WOS:000233655200002. https://doi.org/10.1002/mrm.20729 PMID: 16270331

24. Sanpitak P, Bhusal B, Nguyen BT, Vu J, Chow K, Bi X, et al., editors. On the accuracy of Tier 4 simulations to predict RF heating of wire implants during magnetic resonance imaging at 1.5 T. 2021 43rd Annual International Conference of the IEEE Engineering in Medicine & Biology Society (EMBC); 2021: IEEE.

25. Nguyen BT, Bhusal B, Rahsepar AA, Fawcett K, Lin S, Marks DS, et al. Safety of MRI in patients with retained cardiac leads. Magnetic resonance in medicine. 2021.

26. Vu J, Bhusal B, Rosenow J, Pilitsis J, Golestanirad L, editors. Modifying surgical implantation of deep brain stimulation leads significantly reduces RF-induced heating during 3 T MRI. 2021 43rd Annual International Conference of the IEEE Engineering in Medicine & Biology Society (EMBC); 2021: IEEE.

27. Vu J, Nguyen BT, Bhusal B, Baraboo J, Rosenow J, Bagci U, et al. Machine Learning-Based Prediction of MRI-Induced Power Absorption in the Tissue in Patients With Simplified Deep Brain Stimulation Lead Models. IEEE Transactions on Electromagnetic Compatibility. 2021; 63(5):1757–66. https://doi.org/10.1109/temc.2021.3106872 PMID: 34898696

28. Zheng C, Chen X, Nguyen BT, Sanpitak P, Vu J, Bagci U, et al., editors. Predicting RF Heating of Conductive Leads During Magnetic Resonance Imaging at 1.5 T: A Machine Learning Approach. 2021 43rd Annual International Conference of the IEEE Engineering in Medicine & Biology Society (EMBC); 2021: IEEE.

29. Bhusal B, Jiang F, Kim D, Hong K, Monge M, Webster G, et al. The Position and Orientation of the Pulse Generator Affects MRI RF Heating of Epicardial Leads in Children 2022 44th Annual International Conference of the IEEE Engineering in Medicine & Biology Society (EMBC)2022.

30. Jiang F, Bhusal B, Sanpitak P, Webster G, Popescu A, Kim DB, et al., editors. A comparative study of MRI-induced RF heating in pediatric and adult populations with epicardial and endocardial implantable electronic devices. 2022 44th Annual International Conference of the IEEE Engineering in Medicine & Biology Society (EMBC); 2022.

31. McElcheran CE, Golestanirad L, Iacono MI, Wei PS, Yang B, Anderson KJT, et al. Numerical Simulations of Realistic Lead Trajectories and an Experimental Verification Support the Efficacy of Parallel Radiofrequency Transmission to Reduce Heating of Deep Brain Stimulation Implants during MRI. Sci Rep-Uk. 2019;9. doi: ARTN 2124. PubMed PMID: WOS:000458619600123. https://doi.org/10.1038/s41598-018-38099-w PMID: 30765724

32. Golestanirad L, Kazemivalipour E, Lampman D, Habara H, Atalar E, Rosenow J, et al. RF heating of deep brain stimulation implants in open-bore vertical MRI systems: A simulation study with realistic device configurations. Magn Reson Med. 2020; 83(6):2284–92. https://doi.org/10.1002/mrm.28049 PubMed PMID: WOS:000534576700033. PMID: 31677308

33. Kazemivalipour E, Keil B, Vali A, Rajan S, Elahi B, Atalar E, et al. Reconfigurable MRI technology for low-SAR imaging of deep brain stimulation at 3T: Application in bilateral leads, fully-implanted systems, and surgically modified lead trajectories. Neuroimage. 2019; 199:18–29. https://doi.org/10.1016/j.neuroimage.2019.05.015 PMID: 31096058; PubMed Central PMCID: PMC7266624.

34. Golestanirad L, Iacono MI, Keil B, Angelone LM, Bonmassar G, Fox MD, et al. Construction and modeling of a reconfigurable MRI coil for lowering SAR in patients with deep brain stimulation implants.

Neuroimage. 2017; 147:577–88. https://doi.org/10.1016/j.neuroimage.2016.12.056 PubMed PMID: WOS:000394560600051. PMID: 28011252

35. Golestanirad L, Keil B, Angelone LM, Bonmassar G, Mareyam A, Wald LL. Feasibility of Using Linearly Polarized Rotating Birdcage Transmitters and Close-Fitting Receive Arrays in MRI to Reduce SAR in the Vicinity of Deep Brain Simulation Implants. Magn Reson Med. 2017; 77(4):1701–12. https://doi.org/10.1002/mrm.26220 PubMed PMID: WOS:000398085200034. PMID: 27059266

36. Kozlov M, Turner R. Fast MRI coil analysis based on 3-D electromagnetic and RF circuit co-simulation. J Magn Reson. 2009; 200(1):147–52. https://doi.org/10.1016/j.jmr.2009.06.005 PubMed PMID: WOS:000268964700022. PMID: 19570700

37. Golestanirad L, Rahsepar AA, Kirsch JE, Suwa K, Collins JC, Angelone LM, et al. Changes in the specific absorption rate (SAR) of radiofrequency energy in patients with retained cardiac leads during MRI at 1.5T and 3T. Magn Reson Med. 2019; 81(1):653–69. Epub 2018/06/13. https://doi.org/10.1002/mrm.27350 PMID: 29893997; PubMed Central PMCID: PMC6258273.

38. Kazemivalipour E, Bhusal B, Vu J, Lin S, Nguyen BT, Kirsch J, et al. Vertical open-bore MRI scanners generate significantly less radiofrequency heating around implanted leads: A study of deep brain stimulation implants in 1.2T OASIS scanners versus 1.5T horizontal systems. Magn Reson Med. 2021. https://doi.org/10.1002/mrm.28818 PubMed PMID: WOS:000648014900001. PMID: 33961301

39. Neurostimulatin devices: Market estimation & trend analysis from 2016 to 2024. San Francisco, CA: Grand View Research, Inc. 2016.

40. Calcagnini G, Triventi M, Censi F, Mattei E, Bartolini P, Kainz W, et al. In vitro investigation of pacemaker lead heating induced by magnetic resonance imaging: Role of implant geometry. J Magn Reson Imaging. 2008; 28(4):879–86. https://doi.org/10.1002/jmri.21536 PubMed PMID: WOS:000259791300009. PMID: 18821629

41. Mattei E, Triventi M, Calcagnini G, Censi F, Kainz W, Mendoza G, et al. Complexity of MRI induced heating on metallic leads: Experimental measurements of 374 configurations. Biomed Eng Online. 2008;7. doi: Artn 11. https://doi.org/10.1186/1475-925x-7-11 PubMed PMID: WOS:000254874100001.

42. Nordbeck P, Fidler F, Weiss I, Warmuth M, Friedrich MT, Ehses P, et al. Spatial distribution of RF-induced E-fields and implant heating in MRI. Magn Reson Med. 2008; 60(2):312–9. https://doi.org/10.1002/mrm.21475 PubMed PMID: WOS:000258105800010. PMID: 18666101

43. Nordbeck P, Ritter O, Weiss I, Warmuth M, Gensler D, Burkard N, et al. Impact of Imaging Landmark on the Risk of MRI-Related Heating Near Implanted Medical Devices Like Cardiac Pacemaker Leads. Magn Reson Med. 2011; 65(1):44–50. https://doi.org/10.1002/mrm.22592 PubMed PMID: WOS:000285963500006. PMID: 20806352

44. Yeung CJ, Susil RC, Atalar E. RF heating due to conductive wires during MRI depends on the phase distribution of the transmit field. Magn Reson Med. 2002; 48(6):1096–8. https://doi.org/10.1002/mrm.10310 PubMed PMID: WOS:000179524200027. PMID: 12465125

45. Lucano E, Liberti M, Lloyd T, Apollonio F, Wedan S, Kainz W, et al. A numerical investigation on the effect of RF coil feed variability on global and local electromagnetic field exposure in human body models at 64 MHz. Magn Reson Med. 2018; 79(2):1135–44. https://doi.org/10.1002/mrm.26703 PubMed PMID: WOS:000419134600056. PMID: 28421683

46. Eryaman Y, Akin B, Atalar E. Reduction of implant RF heating through modification of transmit coil electric field. Magnetic resonance in medicine. 2011; 65(5):1305–13. https://doi.org/10.1002/mrm.22724 PMID: 21500259

47. Commission IE. Medical electrical equipment-Part 2–33: Particular requirements for the basic safety and essential performance of magnetic resonance equipment for medical diagnosis. IEC 60601-2-33 Ed 30. 2010.

48. Bhusal B, Nguyen BT, Sanpitak PP, Vu J, Elahi B, Rosenow J, et al. Effect of Device Configuration and Patient's Body Composition on the RFHeating and Nonsusceptibility Artifact of Deep Brain Stimulation Implants DuringMRIat 1.5T and 3T. J Magn Reson Imaging. 2020. https://doi.org/10.1002/jmri.27346 PubMed PMID: WOS:000563311600001. PMID: 32860322

49. Steensma BR, Tokaya JP, Stijnman PRS, Erturk MA, van den Berg CAT, Raaijmakers AJE, editors. Effect of transmit frequency on RF heating of metallic implants. In Proceedings of the ISMRM & SMRT Virtual Conference & Exhibition; 2021.